Significantly Enhanced Magnetoresistance in Monolayer WTe2 via Heterojunction Engineering: A First-principles Study

Journal:	*Nanoscale*
Manuscript ID	NR-ART-05-2018-004391.R4
Article Type:	Paper
Date Submitted by the Author:	02-Nov-2018

Complete List of Authors:	Hu, Lin; Beijing Computational Science Research Center Kang, Lei; Beijing Computational Science Research Center, Yang, Jinlong; University of Science and Technology of China, Department of Chemical Physics Huang, Bing; Beijing Computational Science Research Center Liu, Feng; University of Utah, Department of Materials Science

SCHOLARONE™
Manuscripts

Journal Name RSCPublishing

ARTICLE

Cite this: DOI: 10.1039/x0xx00000x

Significantly Enhanced Magnetoresistance in Monolayer WTe_2 via Heterojunction Engineering: A First-principles Study

Lin Hu[a,b], Lei Kang[a], Jinlong Yang[c], Bing Huang[a,b*] and Feng Liu[b,d*]

Received 00th January 2012,
Accepted 00th January 2012

DOI: 10.1039/x0xx00000x

www.rsc.org/

The large non-saturating magnetoresistance (MR) of bulk WTe_2 is known to be greatly reduced in thin film with decreasing thickness. In this study, based on first-principles calculations, we demonstrate that 2D WTe_2 bonded to graphene, through a WTe_2/graphene van der Waals (vdW) heterojunction, can exhibit a significantly enhanced MR, which can be even larger than that of bulk WTe_2. Moreover, the MR shows a strong stacking-orientation-dependent behavior, which facilitates a tunable MR effect. Our findings illustrate a new route to enhancing the MR of WTe_2 and other 2D semimetals via heterojunction engineering, which is useful for a range of applications in information technology.

Introduction

Magnetoresistance (MR) is defined as the resistance of metals or semiconductors that varies with an applied magnetic field. The materials with large MRs can be used in a variety of electronic and magnetic device applications, e.g., magnetic sensors[1], magnetic memories[2] and hardware devices[3]. In magnetic sensor applications, the data can be read from the magnetic hard disk with an MR read sensor that is extremely sensitive to low magnetic fields[4,5]. There is an increasing demand for MR read sensors with high sensitivity, low energy consumption and low cost.

Semimetals, e.g., graphite, bismuth and bulk WTe_2, typically show very large MRs at low temperatures because charge compensation of electrons and holes leads to an approximate cancellation of the Hall *E* field[6]. Recent experiments have also revealed an extremely large positive MR (XMR) in the bulk WTe_2. There are also some other MR effects, e.g. giant MR (GMR)[7,8] and colossal MR (CMR)[9] effects. These two MR effects often occur in thin-film metals and manganese-based perovskites. Comparing with these very large MR effects (GMR and CMR), ordinary MR effect is a relatively weak effect, and it is found in non-magnetic compounds or elements[10]. The magnetic materials typically have negative MR effect. Positive MR is seen in metals, semiconductors and semimetals. And, the bulk WTe_2 was found to be an XMR material[6], whose MR value is even larger than that of some GMR and CMR materials. This XMR effect can be understood by classical magnetic transport theory of a two-band model[11,12], which is widely used to study the MR of two-carrier conduction. The MR in a material with two kinds of carriers is caused by the difference between their drift velocities in an electric field. And the scattering of carriers should equalize the velocities leading to a vanishing MR. According to this model, the magneto-transport properties of a nearly compensated semimetal can be described by the following expression for the longitudinal resistivity $\rho_{xx}(B)$:

$$\rho_{xx}=\frac{(n\mu_e+p\mu_h)+(n\mu_e\mu_h^2+p\mu_h\mu_e^2)B^2}{e[(n\mu_e+p\mu_h)^2+(p-n)^2\mu_e^2\mu_h^2B^2]},(1)$$

Where n, p, μ_e, μ_h, and B are electron density, hole density, electron mobility, hole mobility and magnetic field, respectively. Subsequently the MR of a semimetal can be written as:

$$\frac{\Delta\rho}{\rho}=\frac{\rho_{xx}(B)-\rho_{xx}(0)}{\rho_{xx}(0)}$$
$$=\frac{(n\mu_e+p\mu_h)^2+\mu_e\mu_h(n\mu_e+p\mu_h)(p\mu_e+n\mu_h)B^2}{(n\mu_e+p\mu_h)^2+(p-n)^2\mu_e^2\mu_h^2B^2}-1,(2)$$

Under the charge compensation condition n=p, the external magnetic field term in the denominator can be neglected as $(n\mu_e + p\mu_h)^2 \gg (p-n)^2{\mu_e}^2{\mu_h}^2B^2$ for the range of B in experiments. In this case, the MR will increase indefinitely without saturation as B increases, i.e., $\Delta\rho/\rho = \mu_e\mu_h B^2$.

According to the two-band model[11,12], the MR of a semimetal is mostly determined by μ_e and μ_h. For a thin-film WTe_2 with reduced thickness, both μ_e and μ_h are expected to decrease, when the crystal thickness becomes smaller than the mean free path and scattering at the surface becomes relevant. For example, $\mu_e$and $\mu_h$will be dramatically reduced from 5,000~10,000 in the bulk to ~1,000 in a six-layer film[13]. Consequently, the MR is reduced from 50000 for the bulk to 10000 for the film ($\boldsymbol{B}$ = 15 T), and this value is expected to be even lower in the monolayer WTe_2[13]. This strong thickness-dependent MR effect will inevitably hinder the use of monolayer (or multi-layers) WTe_2 in nanoscale device applications. Therefore, it is of both fundamental interest and practical importance to increase the MR of a monolayer WTe_2, or 2D semimetal in general by increasing its carrier mobility.

The van der Waals (vdW) heterojunction engineering, formed between two 2D monolayers, is widely applied to tune the electronic and optical properties of 2D materials. For example, a moiré structure of graphene on h-BN forming secondary Dirac points has attracted great scientific attentions[14]. In this study, we propose a general approach of achieving very large MR via the vdW heterojunction engineering. The basic concept is illustrated in Fig. 1. Fig. 1a shows the typical band structure of a semimetal, e.g. the monolayer WTe_2, where the electron and hole pockets coexist at the Fermi surface. Fig. 1b shows the heterojunction made of monolayer WTe_2 and graphene, i.e., WTe_2/graphene. Because of the slightly higher work function of WTe_2 compared to graphene, electrons will be transferred from graphene to WTe_2, which enables a n-type doping for WTe_2 and spontaneously a p-type doping for graphene. Consequently, upon forming the heterojunction, μ_h is determined by graphene and μ_n by WTe_2, respectively.

According to classical transport theory[15-16], with a linear band dispersion, e.g. graphene, the mobility is very high, and the MR scales linearly with the magnetic field (~$\boldsymbol{B}$). In contrast, with a parabolic band dispersion, e.g. the monolayer WTe_2, the MR scales quadratically with the magnetic fields (~$\boldsymbol{B}^2$), but the mobility is relatively low. Therefore, by forming the WTe_2/graphene heterojunction, i.e. a parabolic/linear band-junction, one might combine the advantages of both materials to create a scenario for MR to scale with $\boldsymbol{B}^2$, while at the same time having a high carrier mobility. Here, we consider two extreme cases for strong and weak electron-hole resonance. For the former, we use $MR = \mu_e\mu_h B^2$; for the latter, we use the average MR of WTe_2($\boldsymbol{B}^2$ for parabolic dispersion) and graphene($\boldsymbol{B}$ for a linear dispersion): $\mathrm{MR} = (2\mu_h\mu_e^2B^3 + \mu_e^2B^2 + \mu_hB)/(\mu_e^2B^2 + \mu_hB + 2)$ treating the two layers as two parallel transport channels [more details can be found in Supporting Information]. In general, a given system may behave in between the two limiting cases depending on the degree of electron-hole correlation at the heterojunction. When the electron-hole correlation is very strong, similar to the case of WTe_2[6], a synergetic effect should be dominated; conversely, if the electron-hole correlation is very weak, it is more of a doping effect. Our strategy of this heterojunction engineering by combining the advantages of both materials can be generally effective to enhance the MR effect of 2D materials.

Using first-principles calculations, we show that by forming a vdW heterojunction of WTe_2/graphene, the MR of monolayer WTe_2 can be significantly enhanced by several orders of magnitude, to be even larger than that of bulk WTe_2. Interestingly, the MR of WTe_2/graphene also shows a strong stacking-orientation-dependent behavior, which can be understood in terms of in-plane anisotropy of WTe_2 and affords a tunable MR effect.

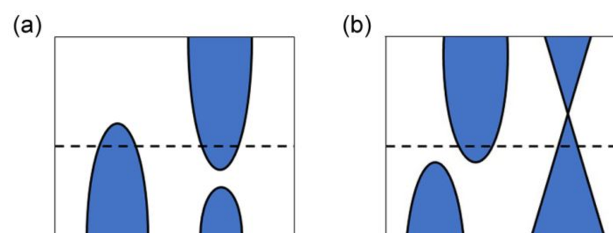

Figure 1. (a) The sketch of band structure of WTe_2 with the coexistence of electron and hole pockets around the Fermi level. (b) WTe_2/graphene heterojunction with electron pocket from the quadratic band of WTe_2 and hole pocket from the linear Dirac band of graphene. The Fermi level is marked by dashed lines.

Results and discussion

For the WTe_2 bulk, our calculated lattice constants, a=6.30Å, b=3.53Å and c=14.10Å, are in good agreement with the previous theoretical results[17] and experimental measurements[13]. Then we used the same method to optimize the structure of WTe_2 monolayer, as exfoliated from the WTe_2 bulk. To simulate the vdW heterojunction, graphene and WTe_2 are modeled using a supercell as illustrated in Fig. 2a-b. We have imposed a commensurability condition between graphene and WTe_2 monolayer, where the lattice constant of a $3\sqrt{3} \times 3$ graphene and a 2×2 WTe_2 can match with each other very well (the lattice mismatch between them is less than 1%).

 This journal is © The Royal Society of Chemistry 2012

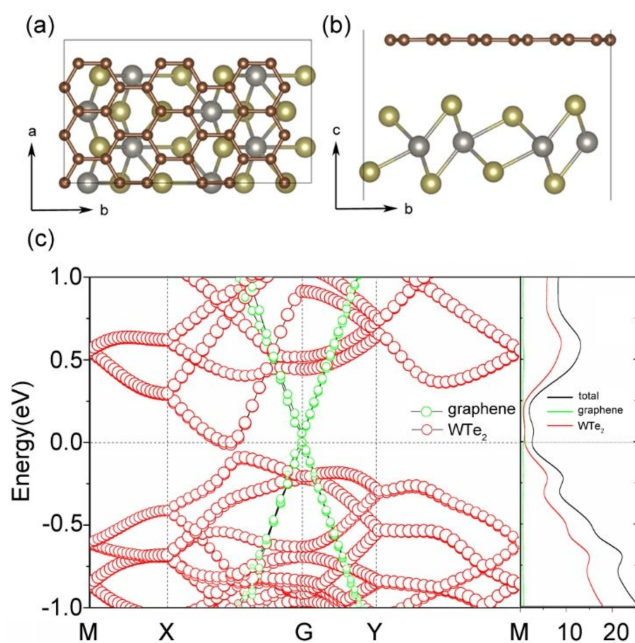

Figure 2. (a) Top and (b) side views of the geometric structures of the WTe_2/graphene heterojunctions. ***a***, ***b*** and ***c*** represent the lattice vectors. The brown, yellow and gray balls represent C, Te and W atoms, respectively. (c) The projected band structure (left panel) and density of states (right panel) of the WTe_2/graphene heterojunction with SOC effect. The Fermi level is set to zero.

After the structural optimization, the interlayer distance of the WTe_2/graphene heterojunction is found to be 3.63Å. The binding energy E_b between the two layers is calculated as:

$$E_b = E_{WTe_2/G} - \left(E_{WTe_2} + E_G\right),(3)$$

Where $E_{WTe2/G}$, E_{WTe2} and E_G are energies of the junction, isolated WTe_2 monolayer and isolated graphene monolayer, respectively. The calculated E_b is -32.5 meV/Å^2. This value is comparable to the recent theoretical result of 2D graphene-based nanocomposites, such as G/h-BN[18], which is the typical vdW interfacial bonding strength.

The calculated electronic band structure of WTe_2 monolayer also agrees well with the previous work[17]. To obtain accurate values of the hole (p-type) and electron (n-type) carrier concentrations, the band-decomposed DOS are calculated. In particular, to calculate the p- (n-) type carrier concentration, we calculate the DOS of the valence (conduction) band and then integrate the DOS from E_F to the valence band maximum (VBM) (conduction band minimum (CBM)). The calculated carrier concentrations, i.e., $p \approx n$=1.57×10^{13} cm^{-2} are in excellent agreement with the previous work of WTe_2 monolayer[17].

Next, we calculated the electronic structure of the WTe_2/graphene heterojunction (Fig. 2c). Due to the very weak interaction of vdW, the band structures of both graphene and WTe_2 are similar to the isolated cases. After the heterojunction is formed, fewer valence and conduction bands are found to cross the Fermi energy, because the overlap of valance and conduction bands in the heterojunction becomes smaller due to band repulsion. The calculated charge distributions of VBM and CBM (see Fig. S1 in the Supporting Information) show that the holes are distributed over the graphene sheets (Fig. S1a), so that VBM takes the shape of a Dirac cone provided by graphene. Meanwhile, the electrons are distributed over the WTe_2 monolayer (Fig. S1b), so that CBM remains still contributed by WTe_2. Due to the different work functions of WTe_2 monolayer (4.45 eV) and graphene (4.40 eV), electrons tend to transfer from graphene to WTe_2 monolayer based on the Schottky-Mott model[19], resulting in weak n-type WTe_2 monolayer and p-type graphene, respectively. This means a strongly enhanced hole mobility in the heterojunction compared with the isolated WTe_2. Furthermore, the charge redistribution may increase the carrier life-time, because the spatial separation of electrons from holes avoids the carrier recombination. Overall, the heterojunction is expected to improve the carrier transport efficiency, while reducing energy loss. For the heterojunction, carrier compensation condition, i.e., the same n- and p-type carrier concentration, is always guaranteed. The calculated carrier concentration for the WTe_2/ graphene is $p \approx n$=1.62×10^{12} cm^{-2}. This charge compensation indicates that there is possibly a non-saturating MR as a function of B in the WTe_2/graphene heterojunction[6,17].

The carrier mobility can be calculated using the deformation potential (DP) model based on the effective mass approximation[20-23]. For a 2D system, it can be expressed as:

$$\mu = \frac{2e\hbar^3 C}{3k_B T (m^*)^2 E_1^2},(4)$$

Here C is the elastic modulus that is defined as: $(E - E_0)/S_0 = C(\Delta l/l)^2/2$. The DP constants E_1 is defined as: $\Delta E/(\Delta l/l)$, ΔE is the energy shifts of the band edges (VBM for the holes and CBM for electrons). $\Delta l/l$ denotes the strain. E_0, S_0 and l_0 are the total energy, cell area and lattice constant (a_0 or b_0) without strain, respectively. T is the temperature and m* is the effective mass. The calculated m*, C and E_1 and μ (at room temperature) are summarized in Table S1. For the WTe_2 monolayer, our results are in good agreement with the previous work[17]. For the WTe_2/graphene heterojunction, the effective mass of hole, contributed by graphene, is almost zero, which cannot be directly calculated by eq. (4). Instead, we use the Boltzman transport theory combined with the deformation potential theory to estimate the hole mobility[22], which have been successfully applied to predict intrinsic carrier mobility of many carbon-based and organic materials, such as graphene, graphene nanoribbon (GNR) and graphdiyne sheet[22]. For the electron mobility mainly contributed by WTe_2, we adopt eq. (4). Comparing the calculated mobility of graphene part in WTe_2/graphene heterojunction with that of isolated graphene. The differences mainly come from the elastic modulus and DP constants, which also verifies that the band structure of graphene dose not change too much, and our results on

graphene are reliable. Since the hole and electron masses are much smaller than those of bulk and monolayer WTe_2, much higher carrier mobilities can be resulted in the WTe_2/graphene heterojunction, which may in turn lead to a larger MR effect in the heterojunction.

Next, we calculated the MR values of WTe_2 bulk, monolayer and WTe_2/graphene heterojunction for comparison. Using Eq. $\Delta\rho/\rho = \mu_e\mu_h B^2$ for strong electron-hole resonance situation, the MR values have been obtained as a function of external magnetic field. The Fig. 3a-b show the MR along both the W-W chains (***a***-direction) and the orthogonal direction (***b***-direction). The MR of bulk is larger than that of WTe_2/graphene heterojunction along W-W chains, whereas in the orthogonal direction, the MR value of the WTe_2/graphene heterojunction is much larger than that of bulk. For both directions, the MR values of the heterojunction are much larger than that of monolayer WTe_2. For weak electron-hole resonance, we use the average MR of WTe_2(B^2 for parabolic dispersion) and graphene(B for a linear dispersion): $\mathrm{MR} = (2\mu_h \mu_e^2 B^3 + \mu_e^2 B^2 + \mu_h B)/(\mu_e^2 B^2 + \mu_h B + 2)$. As shown in Fig. 4a-b, one can see that, in the ***a***-direction (left panel), the average MR of heterojunction is much larger than that of WTe_2 monolayer in a large range of B; in the ***b***-direction (right panel), at the regime of small B (B<3.78T, it is not a small magnetic field in reality), the average MR of heterojunction is also larger than that of WTe_2 monolayer. The real enhancement of heterojunction should be between the two extreme cases we considered. Therefore, we can conclude that the MR effect of heterojunction is significantly increased.

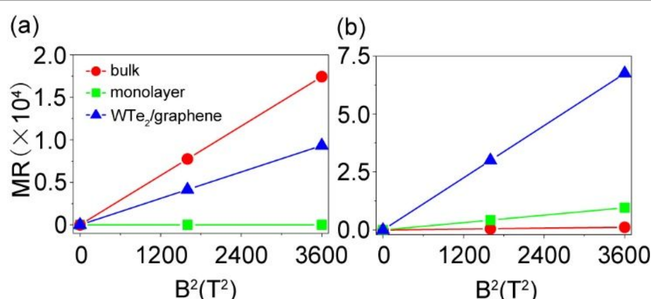

Figure 3. Field dependence of the MR (×10^{4}) in WTe_2 bulk, monolayer and WTe_2/graphene heterojunction along the W-W chains (a) and the orthogonal direction (b), calculated by the equation of $\Delta\rho/\rho = \mu_h\mu_h B^2$.

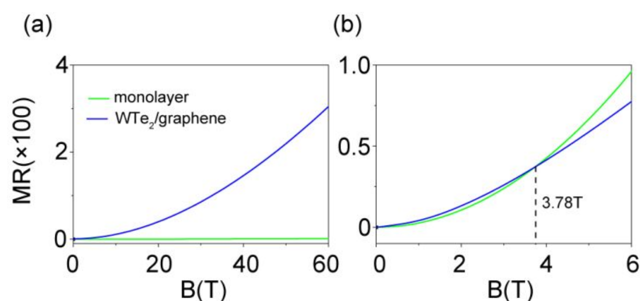

Figure 4. Field dependence of the MR in WTe_2 monolayer and WTe_2/graphene heterojunction along the W-W chains (a) and the orthogonal direction (b), calculated by the equations of $\Delta\rho/\rho = \mu_e\mu_h B^2$ for WTe_2 monolayer and $\Delta\rho/\rho = (2\mu_h\mu_e^2 B^3 + \mu_e^2 B^2 + \mu_h B)/(\mu_e^2 B^2 + \mu_h B + 2)$ for WTe_2/graphene heterojunction.

From Fig. 3 and 4, one sees that the MR of the WTe_2/graphene heterojunction exhibits a strong anisotropy, which results from the fact that electron mobilities along the *b*-axis are much larger than those along the *a*-axis, as shown in Table S1. To understand this anisotropy, we draw the Fermi surface of the heterostructure, as shown in Fig. 5a. One can see that the hole pocket (graphene part) shows an isotropic circle, while the electron pocket (WTe_2 part) is like an American football. This means that the electron mobility anisotropy is indeed contributed by the WTe_2 monolayer.

Another advantage of the vdW heterojunction is that it can form different stacking patterns, which is different from the traditional 3D bulk materials and interface[14]. The MR of the WTe_2/graphene heterojunction exhibits a strong anisotropy. This indicates a strong stacking-orientation-dependent behavior. To verify this point, we define an angle θ to describe the different patterns of stacking between graphene and WTe_2 monolayer. And θ is chosen as the angle between the graphene armchair edge with the ***a*** axis in Fig. 2a. Fixing the WTe_2 monolayer, we rotate graphene to have different stacking angles of θ. Here, we choose two structures with $\theta = 30°$ and $\theta = 10.8°$ as examples. The structures (Fig. S2) and computational details of the results (Table S2) are shown in the Supporting Information. Following the symmetry of graphene, the MR has a period of 60°, and $\theta = 30°$ is the symmetry mirror plane to rotation. Fig. 5b shows the MR as a function of θ. When $\theta = 0°$ or 60°, the MR reaches the maximum value; when $\theta = 30°$, MR reaches the minimum value. MR at $\theta = 60°$ is about 6.3 times larger than that at $\theta = 30°$ at a given external magnetic field (B=14.7T). The MR changes with the angle θ linearly. Thus, we can tune MR up to a few times of difference by changing the stacking angle. Conversely, this provides an alternative method to measure the stacking angle by detecting different MR values.

 This journal is © The Royal Society of Chemistry 2012

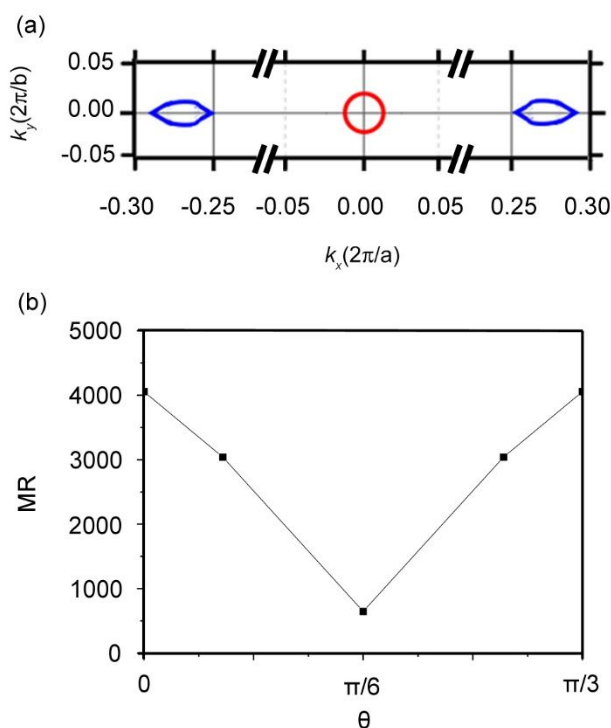

Figure 5. (a) The Fermi surface of WTe_2/graphene. Red and blue circles represent hole and electron pockets, respectively. (b) Dependence of MR of the WTe_2/graphene heterojunction on stacking angle θ for B=14.7T.

Next, we would like to discuss further the condition for electron and hole compensation. In WTe_2/graphene, the work functions of graphene and WTe_2 monolayer are close to each other. Consequently, the shift (ΔE_D) of graphene's Dirac point (E_D) relative to the Fermi level (E_F) is very small ($\Delta E_D = E_D - E_F$). According to the charge carrier (electron or hole) concentration of the doped graphene equation[24,25], $N_{h/e} = (\Delta E_D)^2/(\pi v_F^2)$. When ΔE_D is very small, the carrier concentration change little. However, for a more general case, the difference in work function between the two materials can be larger, so that the two materials have different carrier concentrations, such as in the silicene/graphene heterojunction[26]. Then, the MR effect is reduced and becomes saturated. To overcome this problem, we suggest that interlayer spacing and in-plane strain might be used to possibly restore the carrier compensation condition[26-28].

Conclusions

In summary, we propose an effective approach to enhance the MR of 2D semimetals via vdW heterojunction engineering, and discuss its general physical conditions and applicability. Using density functional theory calculations, we show that charge compensation and non-saturating MR effect may be achieved in the WTe_2/graphene heterojunction. Our findings indicate that the WTe_2/graphene heterojunction may provide an extraordinary MR effect that is even greater than that of bulk WTe_2. Moreover, we find that the magnetoresistance is sensitive to different stack configurations, which provides an effective method to tune the MR with a given external magnetic field. Therefore the WTe_2/graphene heterojunction may afford an attractive material platform for the applications in nanostructured magnetic devices.

Computational method

The first-principles calculations are performed with the Vienna Ab-initio Simulation Package (VASP)[29,30]. The Perdew-Burke-Ernzerhof (GGA-PBE)[31] functional with vdW correction proposed by Grimme (DFT-D2)[32] is used. An energy cutoff of 600 eV is employed for the plane wave basis sets and a vacuum spacing of about 15 Å is used so that the interactions between the layers are negligible. The dipole correction is employed to cancel the errors of electrostatic potential. The k-point sampling uses the Monkhorst-Pack scheme with a 15×15×1 mesh[33]. The criterion of maximum force during optimization on each atom is less than 0.01 eV/Å, and the convergence for the total energy is 10^{-7} eV. The spin-orbit coupling (SOC) has also been taken into account in our calculations.

Acknowledgements

L.H., L.K. and B.H. acknowledge the support from Science Challenge Project (No. TZ2016003), China Postdoctoral Science Foundation (No. 2017M610754), NSFC (Grant No. 11574024 and No. 11704021), NSAF (No. U1530401) and National Key Research and Development Program of China (Grant No. 2016YFB0700700). J.Y. acknowledges financial support from the National Natural Science Foundation of China (Grant No. 21688102) and by the National Key Research & Development Program of China (Grant No. 2016YFA0200604). F.L. acknowledges the support from US-DOE (Grant No. DE-FG02-04ER46148). We also thank Supercomputing Center at USTC, CHPC at University of Utah and Tianhe2-JK at CSRC for providing the computing resource.

Notes and references

[a] Beijing Computational Science Research Center, Beijing 100193, China
[b] Department of Materials Science and Engineering, University of Utah, Salt Lake City, UT 84112, USA.
[c] Hefei National Laboratory for Physical Sciences at the Microscale, Synergetic Innovation Center of Quantum Information and Quantum Physics, University of Science and Technology of China, Hefei, Anhui 230026, China
[d] Collaborative Innovation Center of Quantum Matter, Beijing 100084, China
* E-mail: fliu@eng.utah.edu (F.L.), bing.huang@csrc.ac.cn (B.H.)

Electronic Supplementary Information (ESI) available: [Charge density distributions of VBM and CBM, geometric structures and carrier mobility results for different patterns]. See DOI: 10.1039/b000000x/

1. J. E. Lenz, *Proc. IEEE* 1990, **78**, 973-989.

2. Y. Moritomo, A. Asamitsu, H. Kuwahara and Y. Tokura, *Nature* 1996, **380**, 141-144.
3. J. Daughton, *J. Magn. Magn. Mater.* 1999, **192**, 334-342.
4. S. S. Parkin, C. Kaiser, A. Panchula, P. M. Rice, B. Hughes, M. Samant and S. H. Yang, *Nat. Mater.* 2004, **3**, 862-867.
5. S. Yuasa, T. Nagahama, A. Fukushima, Y. Suzuki and K. Ando, *Nat. Mater.* 2004, **3**, 868-871.
6. M. N. Ali, J. Xiong, S. Flynn, J. Tao, Q. D. Gibson, L. M. Schoop, T. Liang, N. Haldolaarachchige, M. Hirschberger, N. P. Ong and R. J. Cava, *Nature* 2014, **514**, 205-208.
7. W. F. Egelhoff, *et al*., *J. Appl. Phys.* 1995, **78**, 273-277.
8. A. P. Ramirez, R. J. Cava and J. Krajewski, *Nature*, 1997, **386**, 156-159.
9. S. Jin, M. McCormack, T. H. Tiefel and R. Ramesh, *J. Appl. Phys.* 1994, **76**, 6929-6933.
10. F. Y. Yang, *et al*., *Science*, 1999, **284**, 1335-1337.
11. E. H. Sondheimer and A. H. Wilson, P*roc. R. Soc. London Series A Math. Phys. Sci.* 1947, **190**, 435-455.
12. S. S. Murzin, S. I. Dorozhkin, G. Landwehr and A. C. Gossard, *J. Exp. Theor. Phys. Lett.* 1998, **67**, 113-119.
13. L. Wang, I. Gutierrez-Lezama, C. Barreteau, N. Ubrig, E. Giannini and A. F. Morpurgo, *Nat. Comm.* 2015, **6**, 8892.
14. K. S. Novoselov, A. Mishchenko, A. Carvalho and A. H. Castro Neto, *Science* 2016, **353**, 461.
15. M. M. Parish and P. B. Littlewood, *Nature* 2003, **426**, 162-165.
16. A. A. Abrikosov, *Phys. Rev. B* 1998, **58**, 2788-2794.
17. H. Y. Lv, W. J. Lu, D. F. Shao, Y. Liu, S. G. Tan and Y. P. Sun, *EPL* 2015, **110**, 37004.
18. Y. Ma, Y. Dai, M. Guo, C. Niu and B. Huang, *Nanoscale* 2011, **3**, 3883-2887.
19. J. Bardeen, *Phys. Rev.* 1947, **71**, 717-727.
20. J. Bardeen and W. Shockley, *Phys. Rev.* 1950, **80**, 72-80.
21. P. J. Price, *Ann. Phys.* 1981, **133**, 217-239.
22. J. Xi, M. Long, L. Tang, D. Wang and Z. Shuai, *Nanoscale* 2012, **4**, 4348-4369.
23. D. Yu, Y. Zhang and F. Liu, *Phys. Rev. B* 2008, **78**, 245204.
24. Z. Chen, I. Santoso, R. Wang, L. F. Xie, H. Y. Mao, H. Huang, Y. Z. Wang, X. Y. Gao, Z. K. Chen, D. Ma, A. T. S. Wee and W. Chen, *Appl. Phys. Lett.* 2010, **96**, 213104.
25. A. Du, Y. H. Ng, N. J. Bell, Z. Zhu, R. Amal and S. C. Smith, *J. Phys. Chem. Lett.* 2011, **2**, 894-899.
26. W. Hu, Z. Li and J. Yang, *J. Chem. Phys.* 2013, **139**, 154704.
27. C. Si, Z. Sun and F. Liu, *Nanoscale* 2016, **8**, 3207-3217.
28. Y. Wang, C. Cong, W. Yang, J. Shang, N. Peimyoo, Y. Chen, J. Kang, J. Wang, W. Huang and T. Yu, *Nano Res.* 2015, **8**, 2562-2572.
29. G. Kresse and J. Furthmüller, *Comput. Mater. Sci.* 1996, **6**, 15-50.
30. G. Kresse and J. Furthmüller, *Phys. Rev. B* 1996, **54**, 11169-11186.
31. J. P. Perdew, K. Burke and M. Ernzerhof, *Phys. Rev. Lett.* 1996, **77**, 3865-3868.
32. S. Grimme, *J. Comput. Chem.* 2006, **27**, 1787-1799.
33. H. J. Monkhorst and J. D. Pack, *Phys. Rev. B* 1976, **13**, 5188-5192.

TOC:

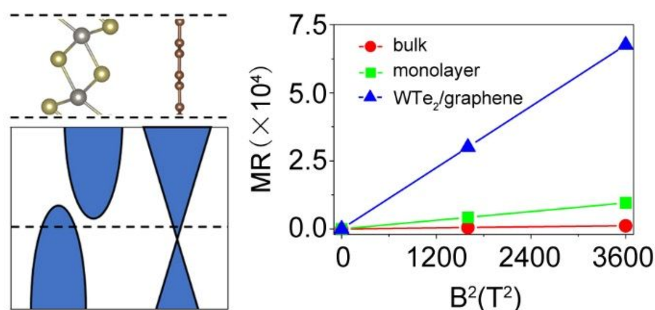

 This journal is © The Royal Society of Chemistry 2012